Nanoscale

Accepted Manuscript

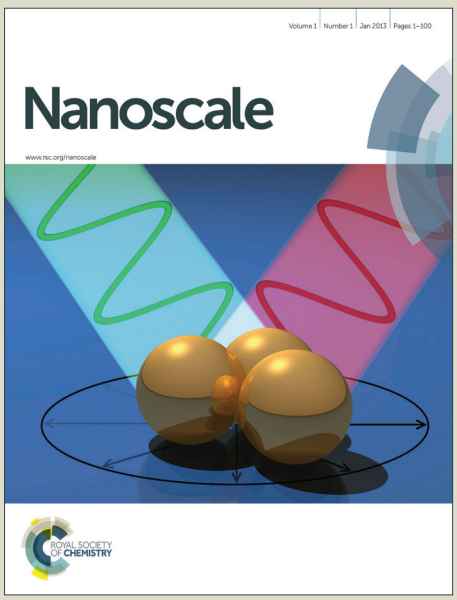

ROYAL SOCIETY OF CHEMISTRY

www.rsc.org/nanoscale

Nanoscale

COMMUNICATION

Visualizing dopamine released from living cells using a nanoplamonic probe

Received 00th January 20xx,
Accepted 00th January 20xx

DOI: 10.1039/x0xx00000x

www.rsc.org/nanoscale

W. W. Qin, [a] S. P. Wang, [a] J. Li, [a] T. H. Peng, [a] Y. Xu, [a] K. Wang, [a] J. Y. Shi, [a b] C. H. Fan[a], D. Li*[a]

We report the development of an ultrasensitive nanoplasmonic probe for discriminative detection and imaging of dopamine released from living cells. The sensing mechanism is based on the dopamine-induced seeded-growth of Au nanoparticles (Au NPs) that leads to shift of plasmon band. This platform allows for the detection of dopamine with a detection limit down to 0.25 pM within 1 min. This nanoplasmonic assay is further applied to visualize the release of dopamine from living Rat pheochromocytoma (PC12) cells under ATP-stimulation with dark-field microscopy (DFM). DFM results together with real time fluorescence imaging of PC12 cells staining with Fluo calcium indicator, suggested that ATP stimulated-release of dopamine is concomitant with Ca^{2+} influx, and the influx of Ca^{2+} is through ATP-activated channels instead of Voltage-gated Ca^{2+} channel (VGC).

Dopamine (DA) is one of the most significant neurotransmitters involved in synaptic communications that transduce information between cells.[1] The process of releasing neurotransmitters that packed in submicrometer-sized vesicle from cells is called exocytosis.[2] Upon the formation of fusion pore of a synaptic vesicle, vesicles release their content into the extracellular space.[3, 4] Thereby, the ability to real time and quantitatively monitoring the dynamic changes of released dopamine offers great opportunities to understand its role in physiological and pathological processes. Several tools have been developed to quantitative analysis of dopamine. Among them, electrochemical methods are dominant because of their real time and online recording advantages.[5-8] Recent development in microelectrode arrays (MEAs) and fast-scan cyclic voltammograms enables recording released neurotransmitter molecules from single cell with nanoscale spatiotemporal resolution and improved molecular resolving power.[9-15] Despite the elegance of these electrochemical techniques, the sophisticated manufacturing of specialized electrodes is crucial, which limits their development.[5] Hence, there is still an urgent need to develop other conceptually new methods to the analysis of released dopamine in exocytosis.[16, 17] Herein, we report a nanoplasmonic approach for quantitative imaging of extracellular dopamine released from living PC12 cells with dark-field microscopy (DFM) and plasmonic Au nanoparticles (NPs).

Localized surface plasmon resonance (LSPR) of coinage metal NPs shows great potential in sensing because of its size and shape, as well as dielectric environment-tunable response.[18-20] For example, Tian et al. developed a colorimetric method for selectively monitoring DA changes in rat brain on the basis of double molecular recognition with 4-mercaptophenylboronic acid (MBA) and dithiobis(succini-midylpropionate) (DSP).[21] The presence of DA induces the aggregation of MBA and DSP co-modified Au NPs, resulting in a red-to-blue color change. However, according to Mie's theory, the scattering cross-section of a spherical particle with radius R much smaller than the wavelength of the light varies as R^6, while its absorption cross-section varies as R^3 only.[22] Therefore, scattering-based detection methods with big Au NPs, in principle, are more sensitive than absorption-based detection. This motivated us to develop new LSPR scattering method for the detection of neurotransmitters with improved sensitivity. Moreover, the optical stability of light scattered from Au NPs enables them as excellent optical probes in imaging. In addition, the advent of dark-field microscopy (DFM) combined with plasmonic resonance Rayleigh scattering (PRRS) spectroscopy[23] provides a powerful means for directly record the LSPR spectrum of single plasmonic NPs, which also enables quantitative measurement.[24, 25] Thereby, the advantage of scattering-based nanoplasmonic assay is its ability to provide both spatiotemporal and quantitative information.

In the present work, we combined the ability of DA to tune PRRS spectra of Au NPs in a seeded-growth process with the advantage of DFM for quantitative imaging to develop an ultrasensitive nanoplasmonic sensor for DA. The nanoplasmonic assay was employed to monitor the release of DA from living PC12 cells under ATP-stimulation. DFM results together with real time fluorescence imaging of PC12 cells staining with Fluo calcium indicator, suggested that ATP-stimulated release of DA is

[a] Division of Physical Biology & Bioimaging Centre, Shanghai Synchrotron Radiation Facility, CAS Key Laboratory of Interfacial Physics and Technology, Shanghai Institute of Applied Physics, Chinese Academy of Sciences, Shanghai 201800, China.
[b] Kellogg College, Oxford University, U.K
E-mail: lidi@sinap.ac.cn
† Electronic Supplementary Information (ESI) available: Figure S1-S4 and Table S1..
See DOI: 10.1039/x0xx00000x

concomitant with a Ca^{2+} influx, and the influx of Ca^{2+} is through ATP-activated channels instead of Voltage-gated Ca^{2+} channel (VGC).

The sensing mechanism is based on a DA-induced seeded growth of Au NPs. DA acts as a reducing agent to reduce $HAuCl_4$ to Au^0 in the presence of Au NPs (50 nm) as seeds. The reduced Au salts are then deposited on Au NPs seeds, which results in a green-to-red change of true scattering color and a redshift of plasmon band (Fig. 1).

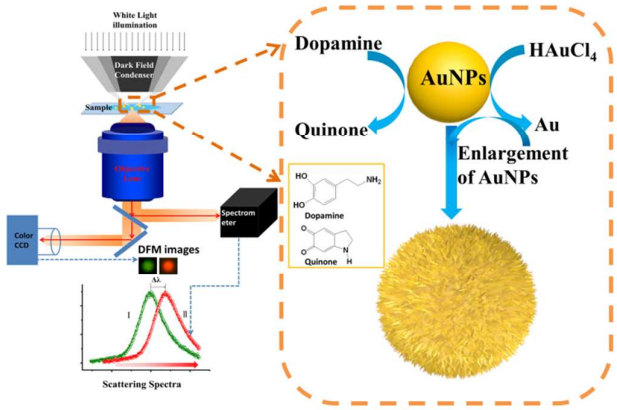

Fig. 1 Schematic illustration the principle of the nanoplasmonic DA sensor.

The concept of bio-catalytic growth of NPs was developed by Willner's group[26-28], and has been extended as a sensing platform for a broad spectrum of biomolecules.[29-32] One limitation of the bio-catalytic growth sensing platform is its poor molecular resolving ability due to the intrinsic redox potential-dependent character.[33] Interestingly, we found that the growth kinetics of Au NPs was different when DA and other catecholamine were introduced as reducing agents. Figure 2A shows the time-dependent plasmon band shift ($\Delta\lambda_{max}$) of Au NPs upon incubating with different growth solutions containing $HAuCl_4$ (0.2 mM) and DA (1 nM), AA (ascorbic acid ,1 μM), CT (catechol, 1 nM), PEA (phenethylamine, 1 nM), TR (tyrosine, 1 nM), EP (epinephrine, 1 nM) and NE (norepinephrine, 1 nM), respectively. The choice of 0.2 mM is an optimized result, it is a turning point of Au source between seeded and non-seeded growth of Au NPs. In the presence DA (1 nM), the growth rate is faster compared with other reducing agents including ascorbic acid of 1, 000 times concentrated. At the initial growth stage of 1 min, $\Delta\lambda_{max}$ induced by DA could be easily differentiated from other analogues (Figure 2B). In addition, the scattering intensity of Au NPs (I) varies as R^6.[22] Therefore, the enlargement of Au NPs not only results in the redshift of plasmon band, but also causes changes of scattering intensity. Figure 2C gives the pattern plot showing the scattering intensity of Au NPs at 580 nm and 560 nm after 1 min of growth. The redshift of plasmon band accompanies an enhancement of I_{580}, while a decrease of I_{560}. DA-treated sample could be clearly isolated from AA and other catecholamine peers. Therefore we chose a growth time of 1 min as the fixed time-interval in further quantitative analysis. Although the precise mechanism underlying the different growth kinetic is still not clear, we postulate that the different pKa and affinity toward Au NPs might play critical role. For example, in neutral pH, DA exists as the positively charged species (pKa1=8.9), while AA exists as the negatively charged one. Therefore, DA is electrostatically attracted by Au NPs, whereas AA is electrostatically repelled by Au NPs, leading to a difference of diffusion constant and growth kinetics.

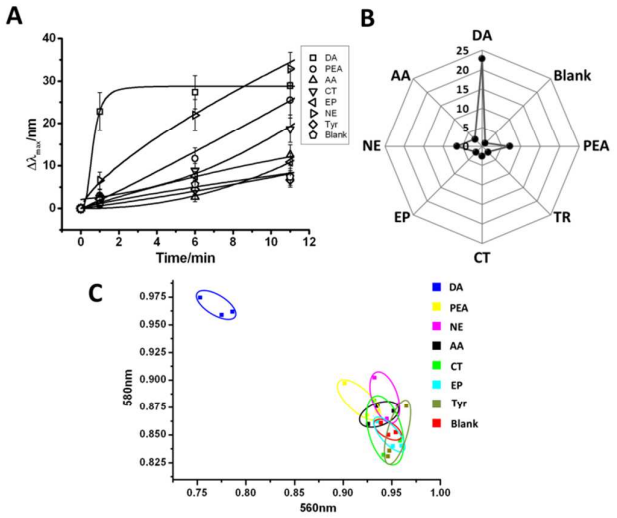

Fig. 2 (A) Time-dependent plasmon band shift ($\Delta\lambda_{max}$) of Au NPs of 50 nm upon treated with different growth solutions containing $HAuCl_4$ (0.2 mM) and DA (1 nM), AA (1 μM), CT (1 nM), PEA (1 nM), TR (1 nM), EP (1 nM) and NE (1 nM), respectively. (B) Radar plot showing the $\Delta\lambda_{max}$ of Au NPs after 1 min of growth upon treated with different reducing agents, listed in (A). (C) Pattern plot showing the scattering intensity of Au NPs at 580 nm and 560 nm after 1 min of growth upon treated with different reducing agents, listed in (A).

We then evaluated the sensing performance with exogenously added DA. Figure 3A shows DFM images of Au NPs upon incubation with growth solutions containing different concentrations of DA (ranging from 0 M to 1 μM) for 1 min. With the increase of DA concentration, we observed a gradual green-to-red color change, indicating the enlargement of AuNPs. The enlargement of Au NPs was also confirmed by scanning electron microscopy (Figure S1). Figure 3B shows the end-point PRRS spectra and the corresponding

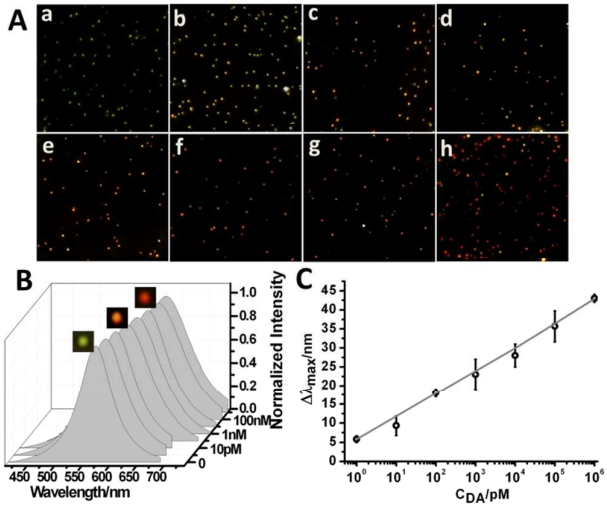

Fig. 3 (A) DFM images of Au NPs upon incubation with growth solutions containing 0.2 mM $HAuCl_4$ and different concentrations of DA: a) 0, b) 1 pM, c) 10 pM, d) 100 pM, e) 1 nM, f) 10 nM, g) 100 nM and h) 1 μM. (B) PRRS spectra of a typical Au NPs upon incubation with growth solutions containing 0.2 mM $HAuCl_4$ and different concentrations of DA. DA concentrations are 0 pM, 1 pM, 10 pM, 100 pM, 1 nM, 10 nM, 100 nM and 1 μM, respectively. The inset images are the true color images of light scattered from single representative Au NPs. C) The derived calibration curve. Error bars represent standard deviations for measurements taken from at least 3 independent experiments.

true color images of a representative Au plasmonic probe after reaction with different concentrations of DA. Similarly, as the concentration of DA was increased, the corresponding λ_{max} was gradually red-shifted. Figure 3C plots the $\Delta\lambda_{max}$ with DA concentration, and LOD was calculated as 0.25 pM (>3σ) (a comparison of LOD of different methods is listed in Table S1).

Having established the plasmonic assay for DA, we employed it to image stimuli-released DA from living cells. PC12 cells have been widely used as a model system of neurosecretion. Previous work revealed that extracellular ATP stimulates catecholamine release.[34] We herein employed this model system to exemplify the proposed nanoplasmonic sensor for imaging stimuli-released DA. Here, we also chose a growth time of 1 min as a fixed time-interval to ensure the selectivity of our strategy. As shown in dark-field image of PC12 cells (Figure 4A(a) and inset), green-color dots were visible before ATP-stimulation. Upon ATP-stimulation and incubation with $HAuCl_4$, orange-color dots were observed (Figure 4A(b) and inset), indicating an enlargement of Au NPs, which confirmed the release of dopamine into the solution. The ATP-stimuli released DA from 1 million cells could be easily distinguished (Figure 4B). Interestingly, we found the stimuli-released DA is Ca2+-dependent (Figure 4C), suggesting the release of DA is concomitant with an influx of Ca^{2+} ions. Ca^{2+} is one of the most important signal transduction elements required in neurotransmitter release.[35, 36] Several pathways are involved in Ca^{2+} influx, including VGC and ATP-activated channels. Thereby understanding the cellular mechanism of coupling Ca^{2+} influx and DA secretion is important because it also clarifies the pathway of Ca^{2+} influx.[37]

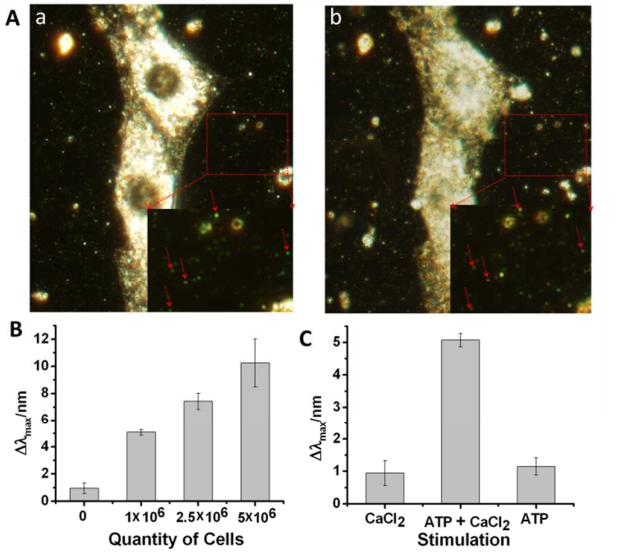

Fig. 4 (A) Dark-field images of nanoplasmonic probes incubated with living PC12 cells (a) and living PC12 cells after ATP(100 μM) stimulation (b) $CaCl_2$ (2 mM) was present in 1 x PBS and 0.2 mM $HAuCl_4$ was added to both systems. Insets of a and b are magnified dark-field images of the representative areas in the red square. (B) Plasmon band shift upon detection of DA that released from different amounts of ATP-stimulated living PC12 cells in ensemble solution. Error bars represent standard deviations for measurements taken from three independent experiments. (C) Plasmon band shift upon detection of DA released from ATP-stimulated living PC12 cells. $CaCl_2$: PC12 cells incubated with 2 mM CaCl2 but without ATP stimulation. ATP + CaCl2: PC12 cells incubated with 2 mM $CaCl_2$ and 100 μM ATP. ATP: PC12 cells incubated 100 μM ATP but in the absence of $CaCl_2$.

We thus introduced a Fluo calcium indicator to stain the stimulated cells, and tried to set the correlation between Ca^{2+} influx and DA release. Figure 5A shows the fluorescence cell images of stained PC12 cell before (a) and after ATP-stimulation (b), while Figure 5B shows the corresponding PRRS spectra (the corresponding DFM images were shown in Figure S2-4). The presence of Ca^{2+} or ATP did not cause notable changes in fluorescence image (Fig. 5Aa and c) and PRRS spectra (Fig. 5Ba and c). Only the co-existence of ATP and Ca2+ brought significant changes in both fluorescence image (Fig. 5Ab) and PRRS spectra (Fig. 5Bb), which further confirmed that the release of DA is concomitant with an influx of Ca2+ ions. When UTP was introduced as an ATP analogue to stimulate the cells, we did not observe detectable changes in fluorescence image (Fig. 5Ad) and PRRS spectra (Fig. 5Bd), suggesting the stimulation is specific to ATP. When Cd^{2+} ions was introduced to block VGC, notable changes in both fluorescence image (Fig. 5Ae) and PRRS spectra (Fig. 5Be) were observed, suggesting the influx of Ca^{2+} is not through VGC. From the above-described fluorescence imaging and PRRS spectra, we concluded that (1) ATP activates Ca^{2+}-permeable cation channels, which leads to an influx of $Ca^{2+}$and further results in a release of DA, (2) the influx of Ca^{2+} is through an ATP-activated channels with ATP receptor instead of VGC.

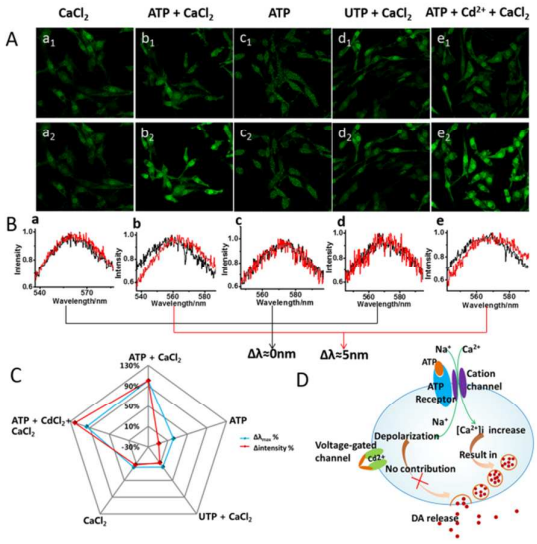

Fig. 5 (A) Fluorescence images of living PC12 cells staining with a Fluo calcium indicator before (top) and after (bottom) stimulation. (B) The PRRS spectra of Au NPs in 1 x PBS before (black) and after (red) the corresponding stimulation. For A and B, a) 2 mM CaCl2, b) 100 μM ATP+2 mM CaCl2, c) 100 μM ATP, d) 100 μM UTP+2 mM CaCl2, e) 100 μM ATP, 300 μM CdCl2, 2 mM CaCl2. (C) The variation of fluorescence intensity and Δλmax (in percentage) corresponds to stimulation in A. (D) Illustration of a hypothetical mechanism of ATP-evoked DA secretion.

Conclusions

In summary, we have developed an ultrasensitive nanoplasmonic sensor for the detection and imaging of DA. DA functions as a reducing agent in a seeded-growth process, leading to a redshift of PRRS spectrum. The plasmonic assay is selective and highly sensitive to DA with a detection limit reaching as low as 0.25 pM with DFM. The proposed plasmonic assay was employed to image stimuli-

released DA from living PC12 cells. DFM results together with fluorescence microscopy suggested that ATP could activate Ca^{2+} influx through an ATP-activated channels with ATP receptor, resulting in a release of DA. Hence, the nanoplasmonic probe exemplifies its ability in quantitative image of neurotransmitters in physiological process through in situ imaging and monitoring its concentration level.

Acknowledgement

This work was supported by the National Basic Research Program of China (973 program, 2013CB933800, 2012CB825800), the National Natural Science Foundation of China ((21222508, 21390414, 61378062, 91313302 and 21329501), and the Shanghai Municipal Commission for Science and Technology (13QH1402) and the Chinese Academy of Sciences.

Notes and references

1. F. Valtorta, R. Fesce, F. Grohovaz, C. Haimann, W. P. Hurlbut, N. Iezzi, F. T. Tarelli, A. Villa and B. Ceccarelli, *Neuroscience*, 1990, **35**, 477-489.
2. T. C. Sudhof, *Annu. Rev. Neurosci.*, 2004, **27**, 509-547.
3. T. C. Sudhof, *Neuron*, 2013, **80**, 675-690.
4. P. W. Kalivas and J. Stewart, *Brain Res. Rev.*, 1991, **16**, 223-244.
5. V. Marx, *Nat. Methods*, 2014, **11**, 1099-1103.
6. R. M. Wightman, *Science*, 2006, **311**, 1570-1574.
7. B. R. Li, Y. J. Hsieh, Y. X. Chen, Y. T. Chung, C. Y. Pan and Y. T. Chen, *J. Am. Chem. Soc.*, 2013, **135**, 16034-16037.
8. M. N. Zhang, K. P. Gong, H. W. Zhang and L. Q. Mao, *Biosens. Bioelectron.*, 2005, **20**, 1270-1276.
9. B. Zhang, M. Heien, M. F. Santillo, L. Mellander and A. G. Ewing, *Anal. Chem.*, 2011, **83**, 571-577.
10. A. Yakushenko, J. Schnitker and B. Wolfrum, *Anal. Chem.*, 2012, **84**, 4613-4617.
11. A. Yakushenko, E. Katelhon and B. Wolfrum, *Anal. Chem.*, 2013, **85**, 5483-5490.
12. J. Wang, R. Trouillon, Y. Q. Lin, M. I. Svensson and A. G. Ewing, *Anal. Chem.*, 2013, **85**, 5600-5608.
13. J. Wang, R. Trouillon, J. Dunevall and A. G. Ewing, *Anal. Chem.*, 2014, **86**, 4515-4520.
14. M. Heien, M. A. Johnson and R. M. Wightman, *Anal. Chem.*, 2004, **76**, 5697-5704.
15. W. Harreither, R. Trouillon, P. Poulin, W. Neri, A. G. Ewing and G. Safina, *Anal. Chem.*, 2013, **85**, 7447-7453.
16. J. J. Deng, P. Yu, Y. X. Wang, L. F. Yang and L. Q. Mao, *Adv. Mater.*, 2014, **26**, 6933-6943.
17. A. Dowd, D. Pissuwan and M. B. Cortie, *Trends Biotechnol*, 2014, **32**, 571-577.
18. J. N. Anker, W. P. Hall, O. Lyandres, N. C. Shah, J. Zhao and R. P. Van Duyne, *Nat. Mater.*, 2008, **7**, 442-453.
19. E. Hutter and J. H. Fendler, *Adv. Mater.*, 2004, **16**, 1685-1706.
20. Y. Li, C. Jing, L. Zhang and Y. T. Long, *Chem. Soc. Rev.*, 2012, **41**, 632-642.
21. B. A. Kong, A. W. Zhu, Y. P. Luo, Y. Tian, Y. Y. Yu and G. Y. Shi, *Angew. Chem. Int. Ed.*, 2011, **50**, 1837-1840.
22. M. A. van Dijk, A. L. Tchebotareva, M. Orrit, M. Lippitz, S. Berciaud, D. Lasne, L. Cognet and B. Lounis, *Phys. Chem. Chem. Phys.*, 2006, **8**, 3486-3495.
23. H. Liu, C. Q. Dong and J. C. Ren, *J. Am. Chem. Soc.*, 2014, **136**, 2775-2785.
24. K. Li, W. W. Qin, F. Li, X. C. Zhao, B. W. Jiang, K. Wang, S. H. Deng, C. H. Fan and D. Li, *Angew. Chem. Int. Ed.*, 2013, **52**, 11542-11545.
25. Y. Zhao, Y. K. He, J. Zhang, F. B. Wang, K. Wang and X. H. Xia, *Chem. Commun.*, 2014, **50**, 5480-5483.
26. M. Zayats, R. Baron, I. Popov and I. Willner, *Nano Lett.*, 2005, **5**, 21-25.
27. I. Willner, R. Baron and B. Willner, *Adv. Mater.*, 2006, **18**, 1109-1120.
28. Y. Xiao, V. Pavlov, S. Levine, T. Niazov, G. Markovitch and I. Willner, *Angew. Chem. Int. Ed.*, 2004, **43**, 4519-4522.
29. L. Zhang, Y. Li, D. W. Li, C. Jing, X. Y. Chen, M. Lv, Q. Huang, Y. T. Long and I. Willner, *Angew. Chem. Int. Ed.*, 2011, **50**, 6789-6792.
30. A. Virel, L. Saa and V. Pavlov, *Anal. Chem.*, 2009, **81**, 268-272.
31. X. X. Zheng, Q. Liu, C. Jing, Y. Li, D. Li, W. J. Luo, Y. Q. Wen, Y. He, Q. Huang, Y. T. Long and C. H. Fan, *Angew. Chem. Int. Ed.*, 2011, **50**, 11994-11998.
32. M. Coronado-Puchau, L. Saa, M. Grzelczak, V. Pavlov and L. M. Liz-Marzan, *Nano Today*, 2013, **8**, 461-468.
33. R. Baron, M. Zayats and I. Willner, *Anal. Chem.*, 2005, **77**, 1566-1571.
34. D. Sela, E. Ram and D. Atlas, *J. Biol. Chem.*, 1991, **266**, 17990-17994.
35. G. J. Augustine, M. P. Charlton and S. J. Smith, *Annu. Rev. Neurosci.*, 1987, **10**, 633-693.
36. M. J. Berridge, *Neuron*, 1998, **21**, 13-26.
37. K. Nakazawa and K. Inoue, *J. Neurophysiol.*, 1992, **68**, 2026-2032.

For TOC only